AN INVESTIGATION OF INTERLAMINAR MATRIX STRESS IN THE VICINITY OF A VOID IN A FIBROUS COMPOSITE MODEL

A THESIS

Presented to

The Faculty of the Division of Graduate Studies

By

Chi-Jen Chen

In Partial Fulfillment

of the Requirements for the Degree

Master of Science in Engineering Science and Mechanics

Georgia Institute of Technology

July, 1976

T-3681-3

AN INVESTIGATION OF INTERLAMINAR MATRIX STRESS IN THE VICINITY OF A VOID IN A FIBROUS COMPOSITE MODEL

Approved:

D. G. Berghaus, Chairman

C. E. S. Ueng

M. S. Raville

Date approved by Chairman 9-2-76

ACKNOWLEDGMENTS

I am much in debt to Dr. D. G. Berghaus, my advisor, for his guidance in all directions. Thanks to Mr. M. G. Turner, who fabricated many of the experimental parts.

Page missing from thesis

LIST OF ILLUSTRATIONS

LIST OF ILLUSTRATIONS (Continued)

SUMMARY

In this report, a $\pm 45^{\circ}$ fiber glass-epoxy two layer composite laminate model containing a void in the region between the fiber layers was built for experimental stress analysis. The scattered light photoelastic technique was used for studying the interlaminar secondary principal stress difference. A region of relatively high stress was produced in the vicinity of the void. Cure, post cure, and viscoelastic problems experienced with the model material hindered the analysis.

CHAPTER I

INTRODUCTION

When high modulus fibers are combined with an organic, ceramic or metal matrix, a composite material is formed. With suitable fiber orientation in a matrix, this results in an increase in structural efficiency of the material. More recently fiber reinforced resin composites have become important in material applications for their strength to weight and stiffness to weight advantages. Laminated composites [1] may consist of layers of different materials. Such layered construction has been used widely in fiber reinforced composites.

Special problems are associated with stress analysis in fibrous composite materials. In a theoretical stress and strain analysis of laminated composites, it is often assumed that each layer is anisotropic but homogeneous. For such analysis, a generalized Hooke's law [2] is used

$$\sigma_i = C_{ij}\varepsilon_j \qquad i,j = \ldots,6 \tag{1}$$

where σ_i are the stress components, C_{ij} is the stiffness matrix, and ε_j are the strain components for the presumed homogeneous material. Such analyses do not admit the heterogeneous nature of the composite structure as consisting of distinctly separate constituents. The stiffness of the laminate is obtained from the properties of the individual laminae, with principal directions oriented at given angles to the

chosen axes of the laminate as shown in Figure 1.

According to classical lamination theory [3], the resultant force and moment on a laminate have the following relationship with the laminate middle surface strain ϵ° and curvatures κ in each layer as

$$\begin{Bmatrix} N \\ M \end{Bmatrix} = \begin{bmatrix} A & B \\ B & D \end{bmatrix} \begin{Bmatrix} \epsilon^{\circ} \\ \kappa \end{Bmatrix} \tag{2}$$

where N is the resultant force and M is the resultant moment. [A] is called extensional stiffness, [B] is coupling stiffness and [D] is the bending stiffness.

Equation (2) permits calculation of the theoretically defined stresses σ_x, σ_y, τ_{xy} in the plane of laminate using appropriate stress-strain and stress versus bending curvature relationships, but no account is taken for interlaminar stresses such as σ_z, τ_{zx}, τ_{zy}. These interlaminar stresses are considered to be one of the causes of failure in composite materials.

CHAPTER II

INTERLAMINAR STRESS-DELAMINATION

Pipes and Pagano [4] have theoretically investigated the interlaminate stresses in a cross-ply laminate under uniform axial extension. Pipes and Daniel [5] used the Moiré fringe method to demonstrate the physical existence of interlaminar stresses at the free edge of laminate. The interlaminar shearing stresses were found to be high and they are therefore considered to be a cause of the debonding problem or delamination. Belanger [6] pointed out that delamination is attributed to poor interlaminar shear strength of the composite. These investigations have shown the importance of interlaminar stresses in multilaminar composites.

CHAPTER III

VOIDS AND DEBONDING

As mentioned above, interlaminar stresses greatly influence debonding and failure in composite materials. It is furthermore known that voids, consisting of air bubbles entrapped in the matrix during composite fabrication, have a significant effect on the composite properties even if the bubbles occupy a small amount of the material volume [7]. Interlaminar shear strength is reduced [8] as is the resistance to environmental degradation [9]. A variety of experimental procedures for measuring the size of voids has been evaluated and applied to a group of graphite-epoxy laminates [10]. Strong emphasis has been given to developing manufacturing processes to minimize inclusion of voids [11]. The effect of an air void trapped at various positions along the fiber-matrix interface was investigated by Owen and Lyness [12] for the case of a single fiber model. High stresses are produced at the interface. Kavanagh [13] studied the effects of geometric variables associated with voids on the evaluation of mechanical properties. Williams [14] examined a different theory for studying stresses in the vicinity of void. He pointed out the difference in stress results (adjacent to a void) which are associated with selection of eigenfunctions of the characteristic equation. He suggested the use of energy methods and further suggested the application of the methods to certain types of adhesion problems.

In this report, fabrication of a two layer $\pm 45^{\circ}$ of glass fiber composite model is described. The interlaminar secondary principal stress difference in a plane parallel to the load direction and in the vicinity of a single specially fabricated void in the central region of a composite model is studied. The scattered light photoelastic method is used.

CHAPTER IV

EXPERIMENTAL SOLUTION METHOD USING A PHOTOELASTIC MODEL

Consider a two layer $\pm 45^{\circ}$ fiber glass composite model with a void between the layers as shown in Figure 2. Fiber layers are parallel to the xy-plane, and a uniformly distributed tensile load is applied in the X-direction in an XYZ Cartesian coordinate system.

Experimental methods have been applied for investigating composite models. Daniel, Rawlands and Post [15] used Moiré techniques to determine the strain fields in filamentary composite laminate. The specimens they used were glass-epoxy and boron epoxy with holes and crack existing. They assumed that the material has anisotropic, and inelastic properties. Dalley and Alfrevich applied [16] birefringent coating to an orthotropic-glass fiber reinforced plastic model. Pipes and Dalley [17] also used the birefringent coating method with a graphite epoxy structural laminate for measuring laminate surface strain. However, these techniques are not able to discern effects which vary spatially with location of the composite constituents. Sutliff and Pih [18] used scattered-light photoelasticity to study the stress field in the matrix in the vicinity of a discontinuous single fiber. They demonstrated that the stresses in such a composite model could be successfully investigated using the scattered-light technique. For determining interlaminar shear stresses in a fiber composite laminate model, Berghaus and Aderholdt [19] also used scattered-light photoelasticity

to determine stresses in the matrix of two layer and four layer fibrous laminates. These models considered the composite as a heterogeneous structure. The study in this report uses the assumptions and techniques associated with the heterogeneous structures [19].

In scattered-light photoelasticity [20], the data yield the secondary principal stress difference

$$p' - q' = f \frac{dn}{ds} \tag{3}$$

where p' and q' are the secondary principal stresses [21] in the plane normal to the light beam, f is the material fringe constant, n is the scattered-light fringe order, s is the light propagation direction as shown in Figure 3.

When the light beam is passed in Y-direction [22] in the model as shown in Figure 4

$$\tau_{xz} = \frac{1}{2} (p' - q')_Y \operatorname{Sin} 2\theta_Y = \frac{1}{2} f \frac{dn}{dY} \operatorname{Sin} 2\theta_Y \tag{4}$$

where θ_Y is the location of the maximum secondary principal stress direction [23] with respect to the Z axis. The fringe derivative can be obtained along the light beam by using a smoothed cubic spline [24]. Discrete values of principal direction θ can also be approximated continuously by a suitable function [23]. For the light beam passed in the Y direction it is necessary to view the light beam parallel to the XZ plane.

CHAPTER V

MODEL FABRICATION

A room temperature curing epoxy [24] was chosen for the matrix material in this two layer model. Flint glass rods were selected for the fibers. The room temperature epoxy consists of three main components, with ratios of two pbw ERL 2774 and two pbw 2795, one pbw ZZL 0803*. Cab-o-sil silica gel** was added to the mixture to increase the clarity of the scattered-light fringes. Five milliliters per pound of mixture were used. In order to get a strong glass-resin bond, the glass rods were cleaned as previously [19].

After assembling the mold with fibers in position, the epoxy was mixed for one hour. The bubbles introduced through mixing were evacuated. The mixture was poured into the mold carefully to avoid introducing any air bubbles into the mold especially in the interlaminar layer which the scattered light beam passed through. The epoxy in the lower layer was cured at room temperature for 96 hours. The void was molded then poured and cured for another 96 hours. (Poor void molding techniques prevented a void from being used which was molded simultaneously with the lower fiber layer.) Then the void was cemented to the lower fiber-epoxy layer. After the cement was cured similarly at

*ERL 2774, ERL 2795, ZZl 0803 are trade marks of Union Carbide Corporation, New York, New York.

**Cab-o-sil is a trade mark of the Cabot Corporation, Boston, Massachusetts.

room temperature, the epoxy was poured and cured in the upper layer for a final 96 hours. The model was then removed from the mold and post cured at 105°F for 96 hours. The complete molding sequence is shown in Figure 5.

CHAPTER VI

DATA COLLECTION

The model was submerged in immersion fluid. A Helium-Neon laser light source and a versatile scattered-light polariscope [19] were used to obtain the data.

A uniformly distributed tensile load was applied through load distribution bars in the model. The loading frame was instrumented to monitor the applied load. To remove initial thermal stresses which were evidently introduced during cure and post cure of this model due to the different thermal coefficients of expansion of the glass and epoxy, the model was heated to 115^{o}F. This temperature is below the glassy-rubbery transition temperature for this material.

After the model was slowly heated to 115^{o}F, the tensile load was applied. It was noticed that the load frame strain gage reading dropped suddenly although a temperature compensating strain gage was used. The fringe pattern in the interlaminar layer did not change even as the load, as seen in the strain gage indication, was reduced.

The fringes were observed by viewing normal to the light beam (Y direction) as shown in Figure 6. Fringes were photographed in various directions as previously [19] described. They are shown in Figure 7. Fringe clarity was used in an attempt to determine the secondary principle directions. Smoothed splines with parabolic extrapolation were used as previously [19] to determine fringe

derivatives. A digital computer program was used for calculations.

CHAPTER VII

RESULTS AND CONCLUSIONS

The fringe derivative results and the secondary principal stress difference $\sigma_p' - \sigma_q'$ at different locations are plotted in Figure 8. It is noticed that the peak value of fringe derivative shifts toward the void as the light beam is moved toward the void. In other words, the secondary principal stress difference peak value moves towards to the void as the light beam is moved toward the void. Due to material viscoelastic effects, the maximum principle stress axes could not be determined, therefore the interlaminar shear stress τ_{xz} could not be determined either.

There then appears to be a local region of high stress caused by the void. This region is adjacent to the void in sections normal to the load which pass through the void, but in the material between the void and the loaded edge of the model, this region moves away from the void toward the side edges of the model as the sections approach the loaded edge of the model. There are lower stresses to either side of the high stress region in these sections. This effect may be seen in Figure 8.

Further work with such composite models should be preceded by a study of the molding problems associated with the matrix epoxy. These problems include the cure and post cure time and temperature cycles, the difference in thermal coefficients of expansion for

the matrix and fiber materials and the apparent viscoelastic behavior.

APPENDIX A

CALIBRATION OF MATERIAL USING A CIRCULAR DISK

The stress optical material constant was determined using circular calibration disks loaded as shown below. For such a circular disk, the difference between principal stresses in the plane of the disk at the center of the disk is [27]

$$\sigma_1 - \sigma_2 = \frac{8P}{\pi td} \tag{5}$$

where P is applied load, t = thickness, d = diameter

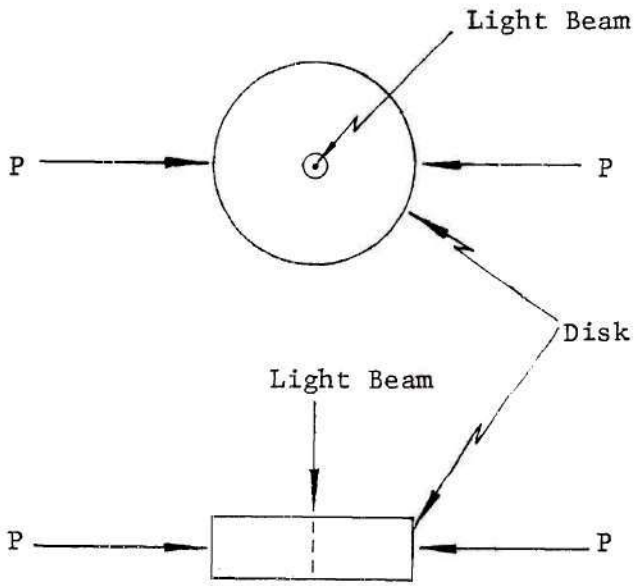

For scattered-light photoelasticity, the principal stress difference, $\sigma_1 - \sigma_2$, is related to the material fringe constant as

$$\sigma_1 - \sigma_2 = f \frac{dn}{dt} \tag{6}$$

from equations (5) and (6), f can be solved for material fringe, f, can be determined. ($f = 100.43$ fringe-psi-in for the material used in this investigation.)

In this material calibration, the epoxy disks were made of the same material as the top and bottom layers of the model. These two circular disks were heated to 115°F in the immersion tank for scattered-light photoelastic investigation as was the two layer $\pm 45^{\circ}$ composite laminate model did. Accumulated fringes through the disk were counted when a diametral compressive load was applied. The number of fringes was divided by the disk thickness to obtain the fringe derivative. A strain gage was mounted on the disk loading frame, and was used to monitor load.

APPENDIX B

FIGURES

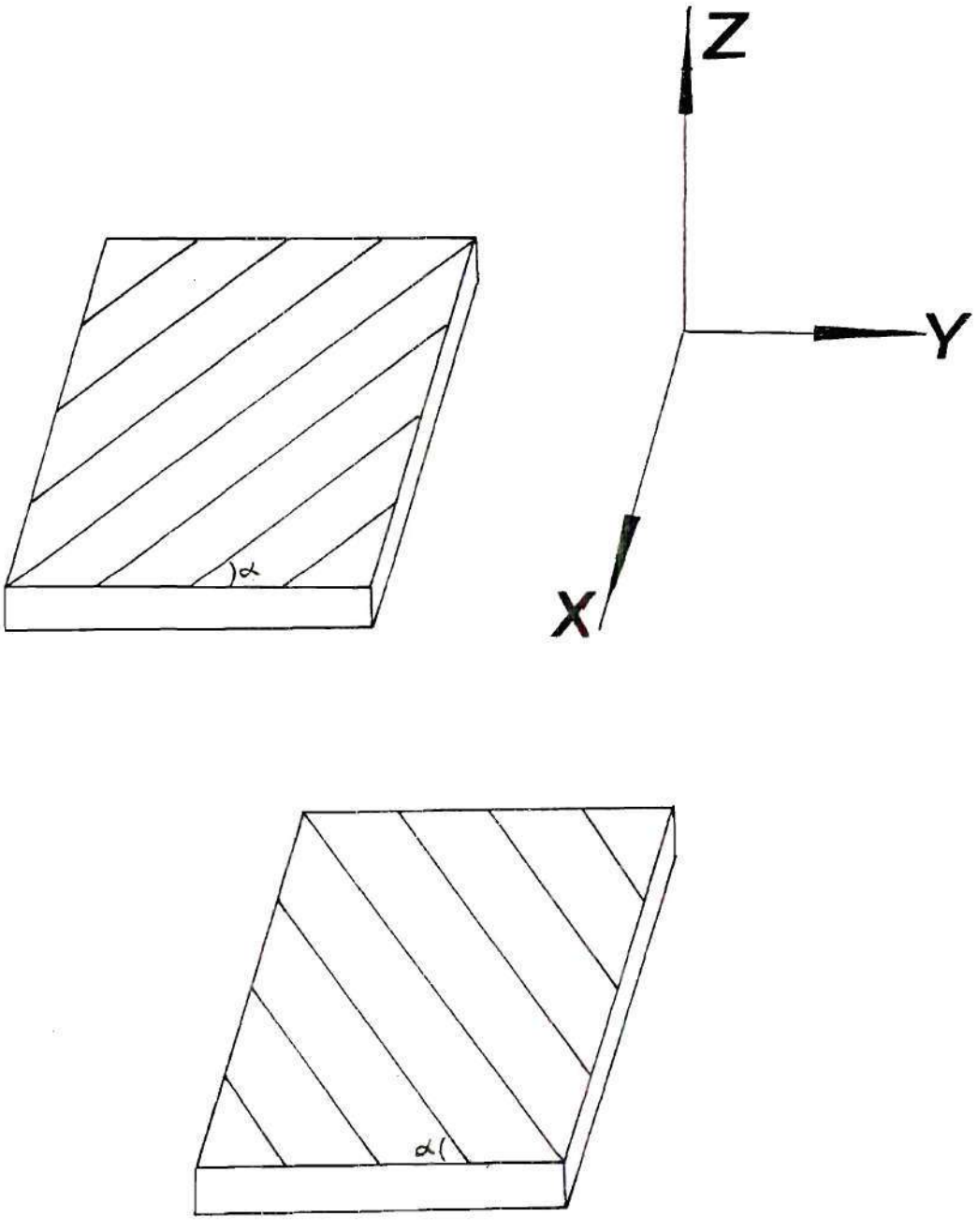

Figure 1. Unbonded View of a Two Layered Antisymmetric Angly-ply Laminate. α is the Angle of Fiber Orientation with Respect to Y Axes.

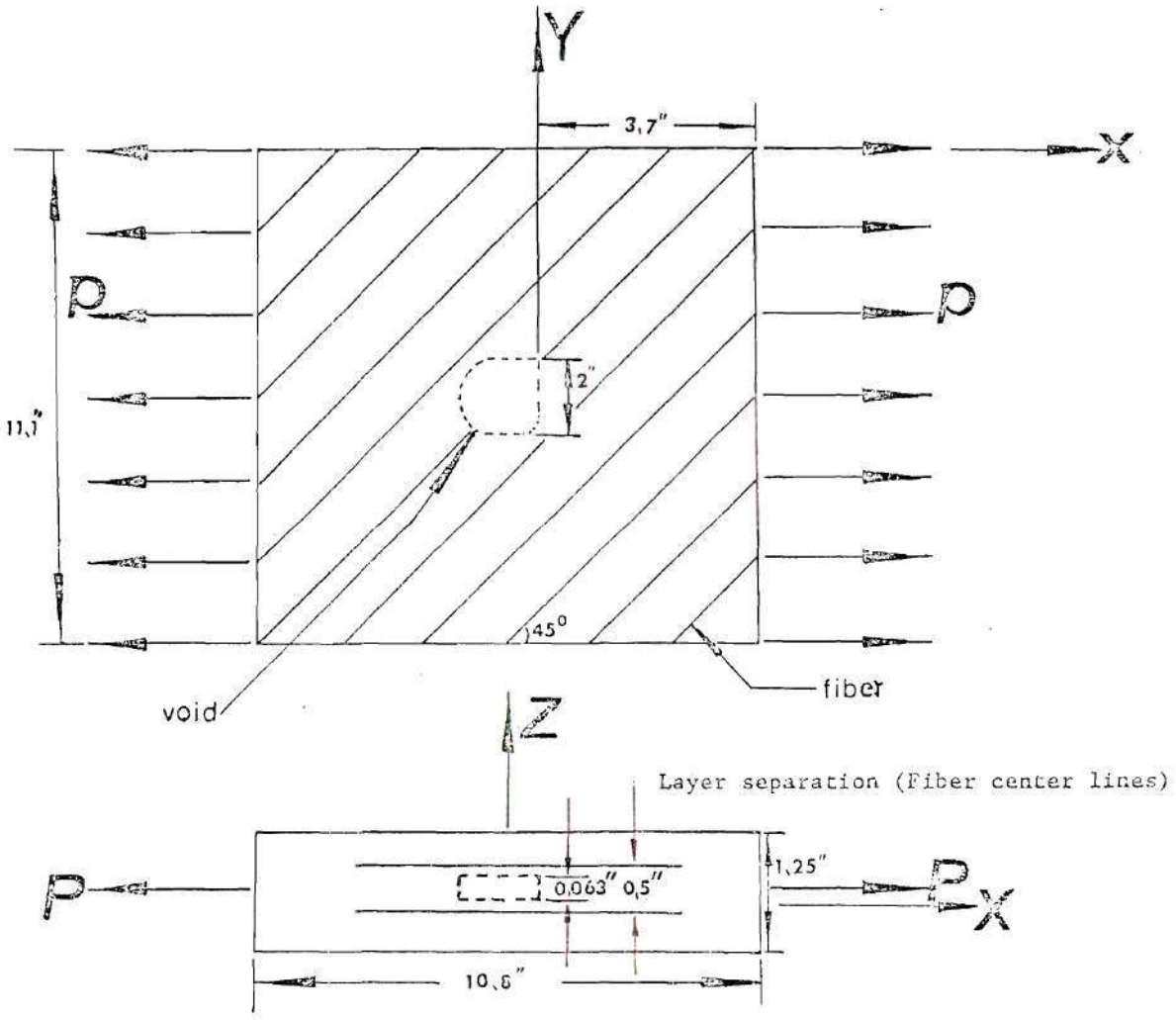

Figure 2. Configuration of Two-Layer Model with Void in Central Region.

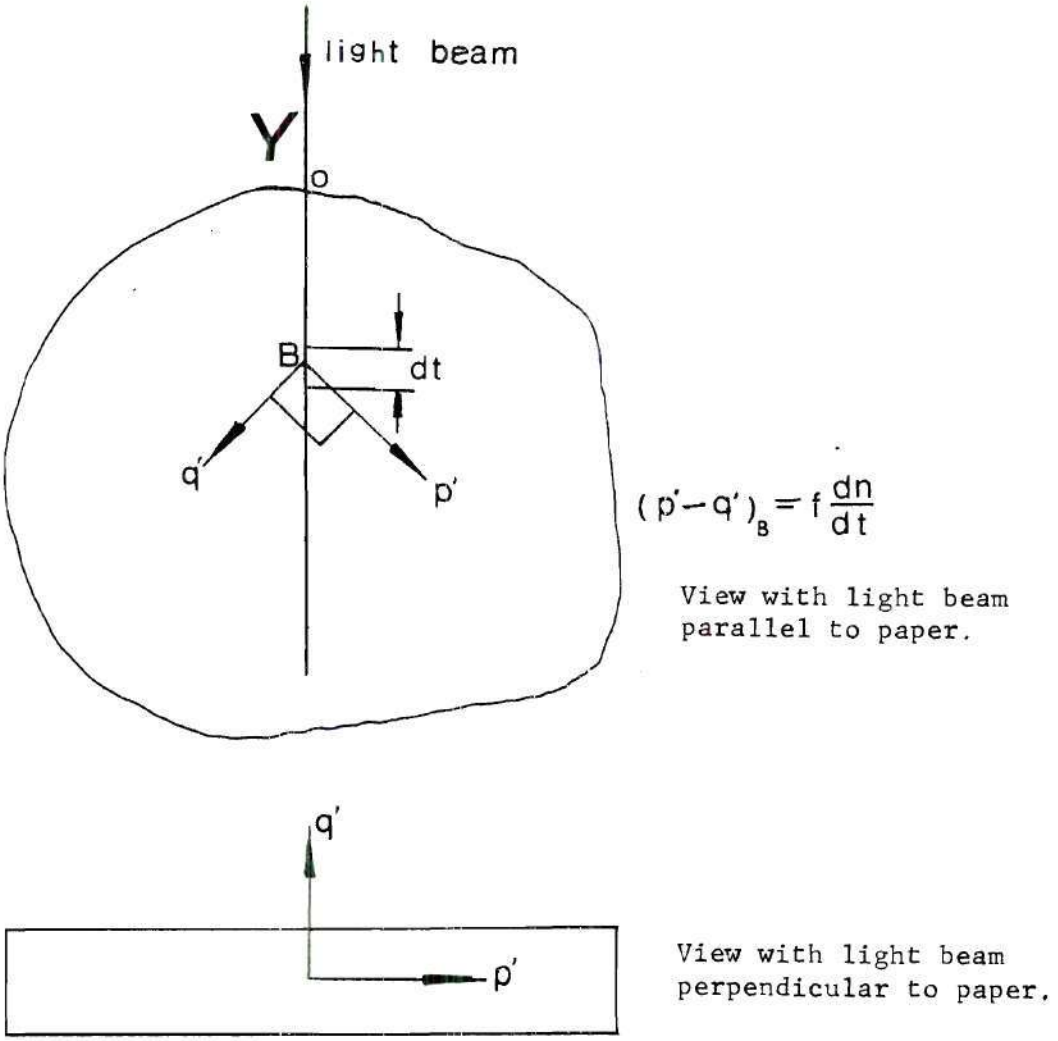

Figure 3. Stress-optical Law for Scattered Light Photoelasticity in Equation (3). p' and q' are Secondary Principal Stresses in Planes Normal to the Light Beam which is Passed in the Y Direction.

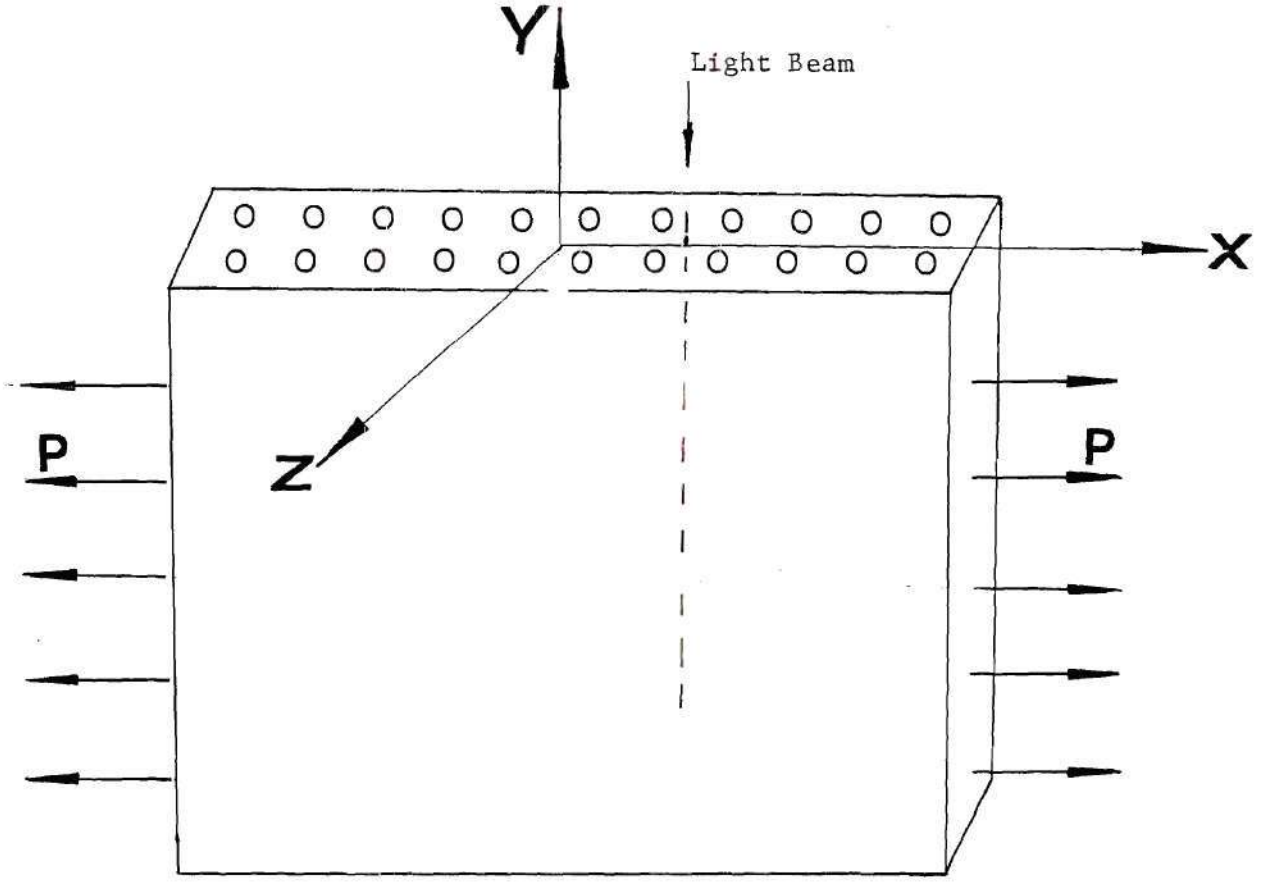

Figure 4. Light Beam Passed through Interlaminar Region for Secondary Principal Stress Difference.

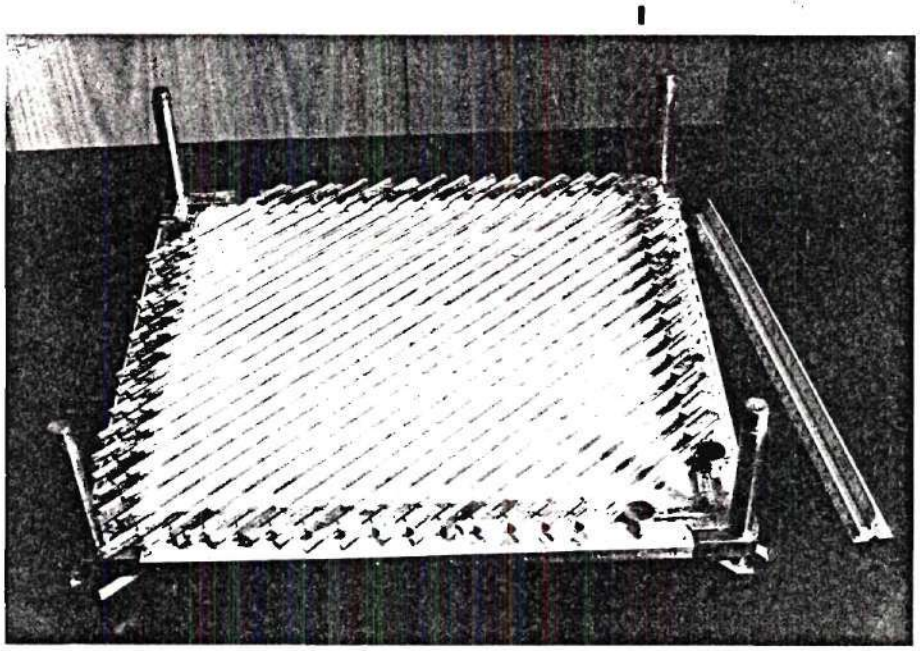

Figure 5a. Glass Fibers in Position for Lower Layer.

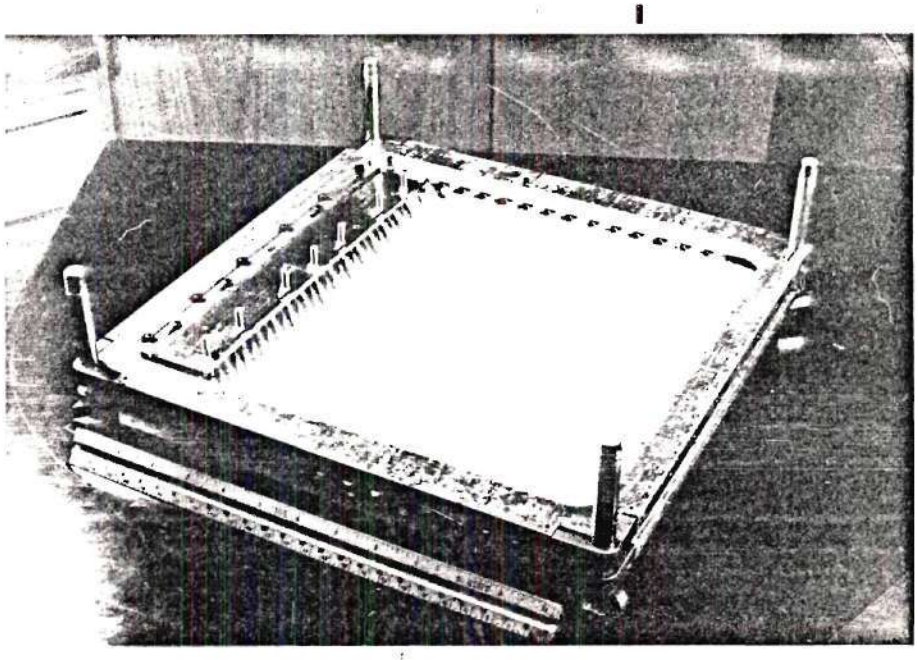

Figure 5b. Uniform Load Distribution Bar in Place in Left Side of Mold.

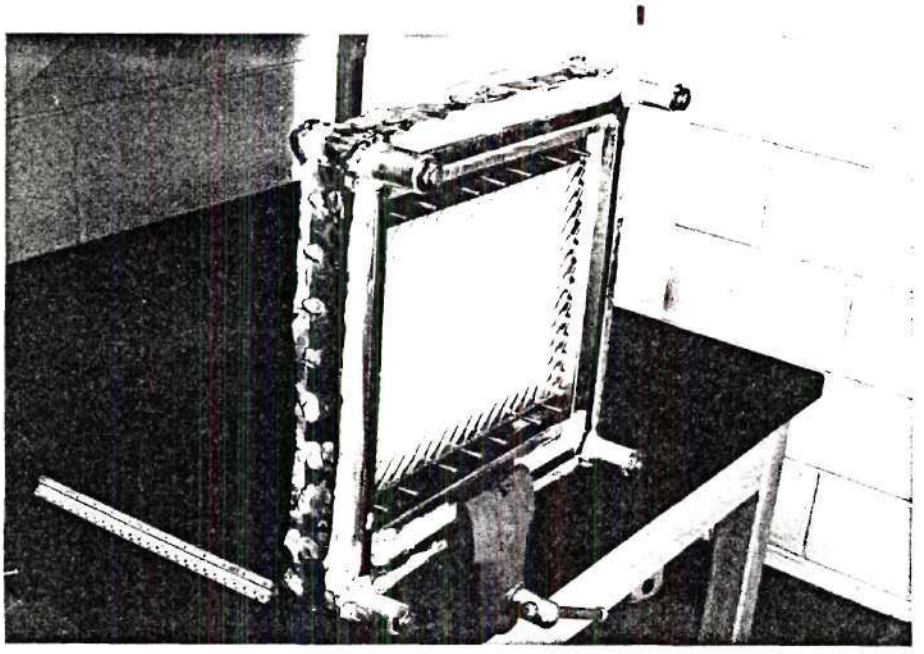

Figure 5c. Mold Sealed with Shim Stock and Clay for Pouring Silicone Rubber Sidewalls.

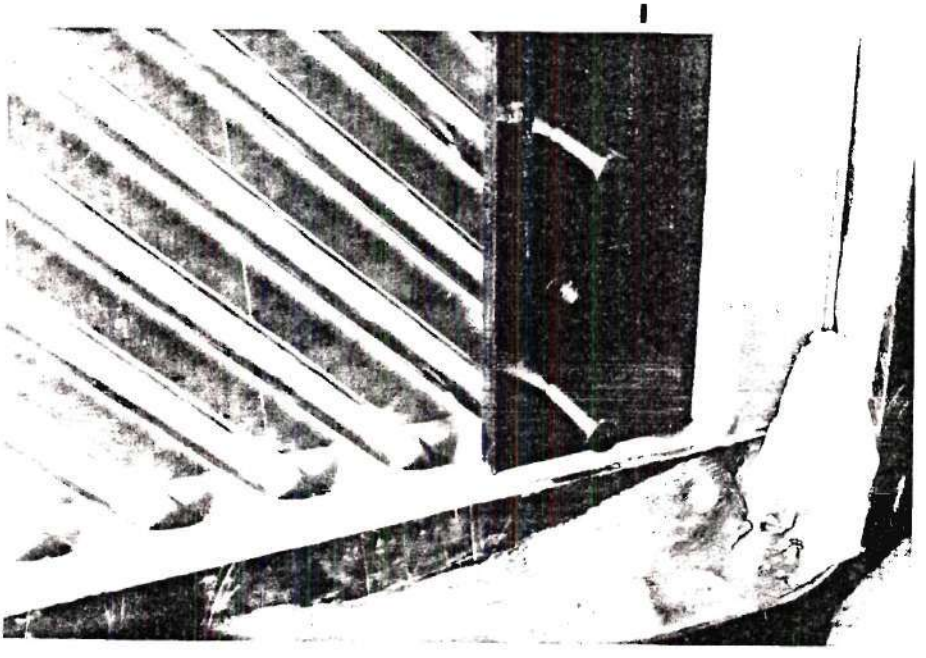

Figure 5d. Close View of Silicone Rubber Along Edges.

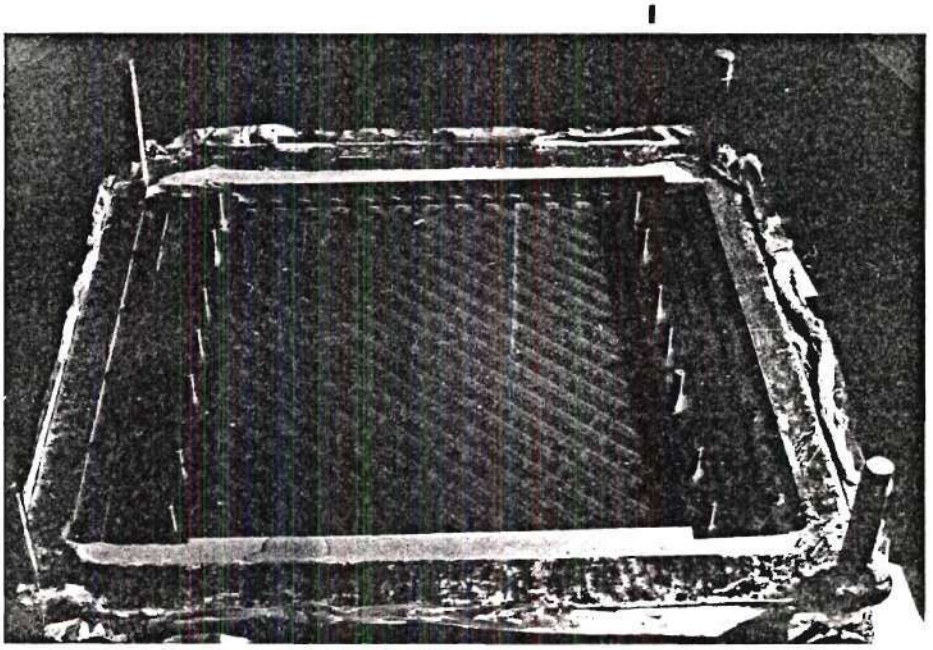

Figure 5e. First Layer Resin Ready for Room Temperature Curing.

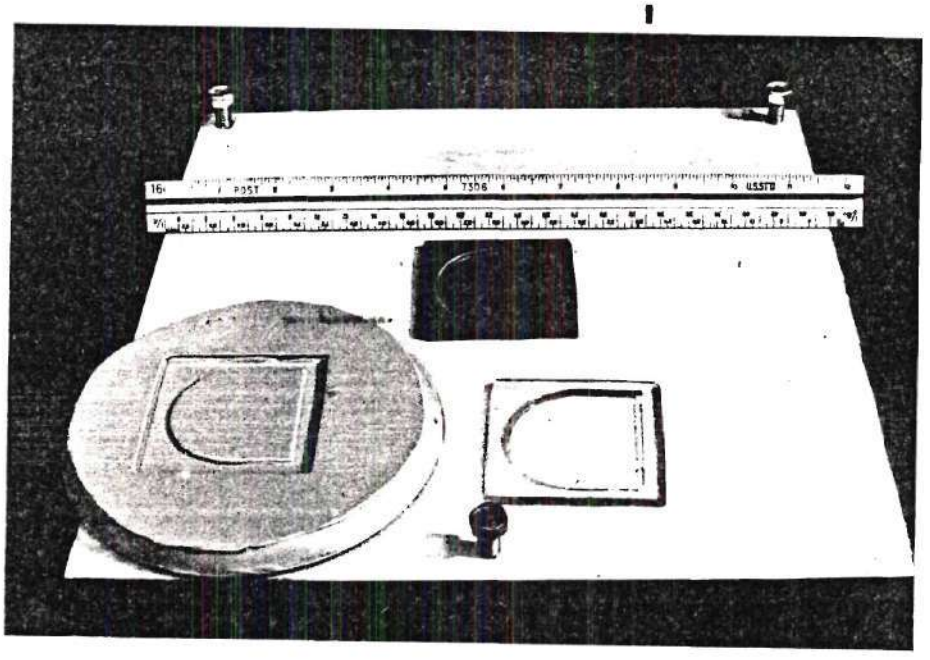

Figure 5f. Void Mold (left), Void Pattern (top), Void (right).

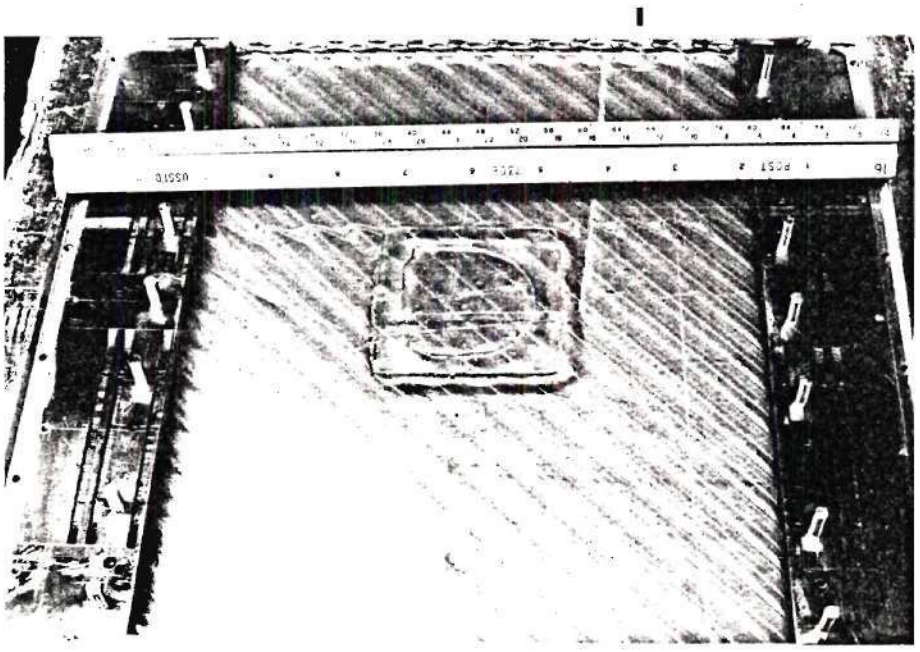

Figure 5g. Void Cemented in Place.

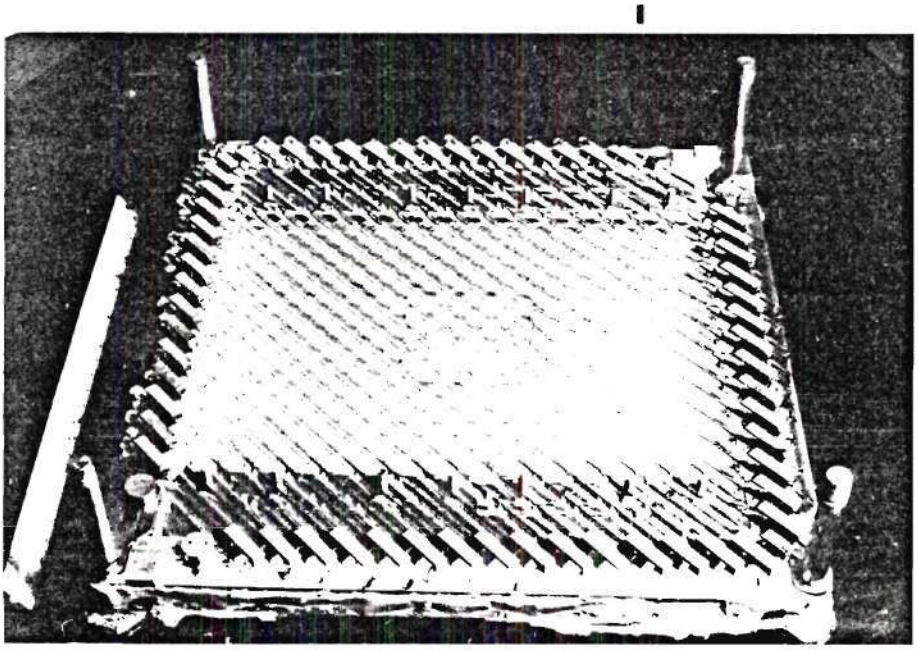

Figure 5h. Fibers in Place for Second Layer.

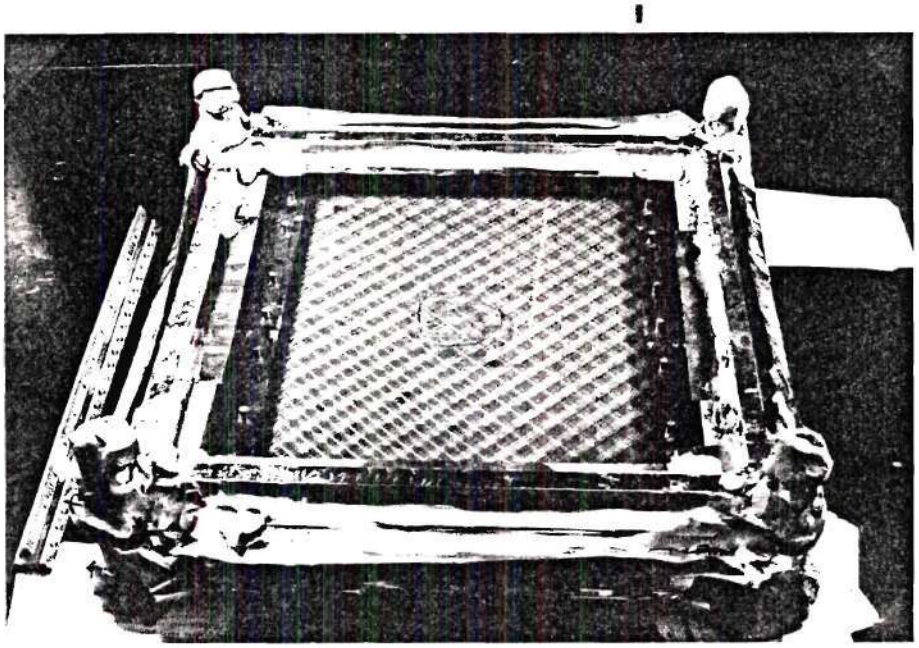

Figure 5i. Second Layer Epoxy during Curing.

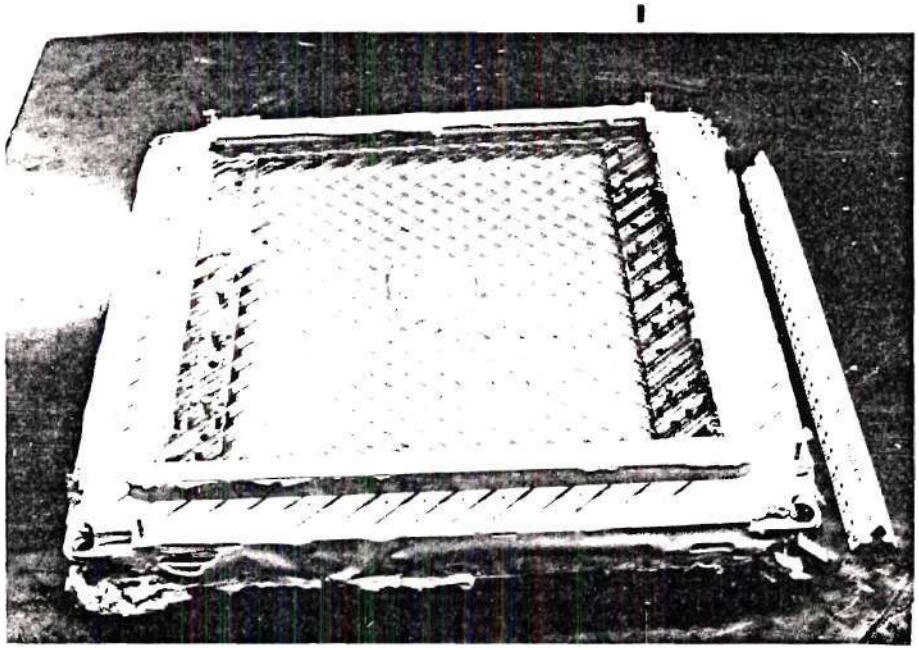

Figure 5j. Completed Model with Mold Frame Removed.

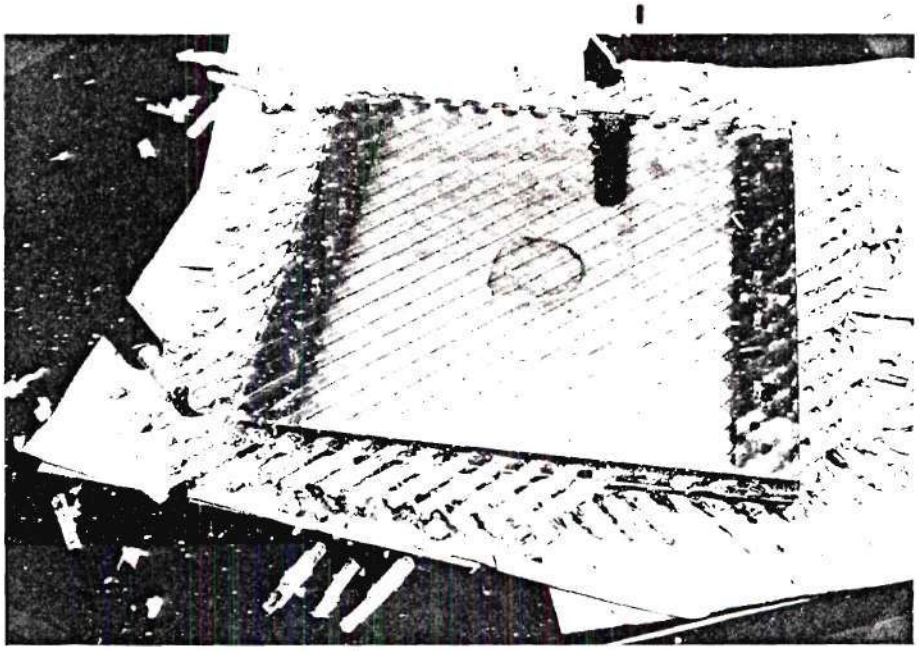

Figure 5k. Removal of Rubber and Fiber Ends.

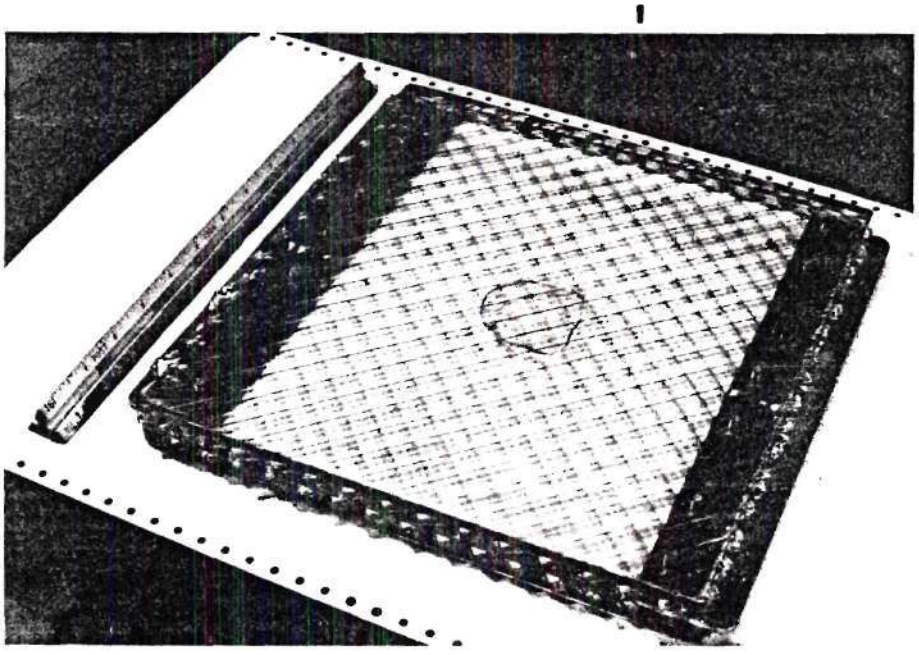

Figure 5ℓ. Two Layer $\pm$ 45° Fiber Glass Laminate with Void in Interlaminar Region; Model Completed.

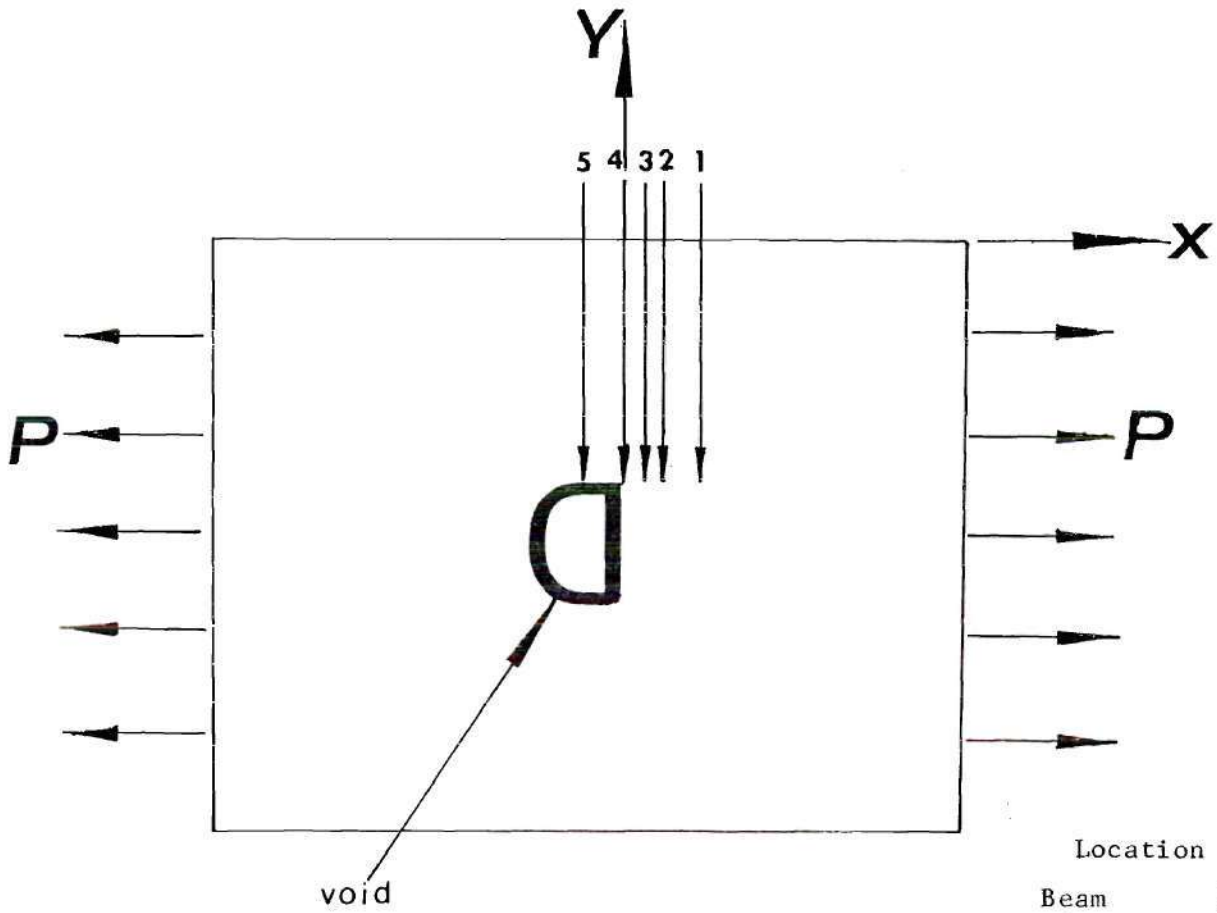

Location

Beam	X
5	-0.5"
4	0
3	0.25"
2	0.5"
1	1.0"

Figure 6. Light Beam at Different Locations for Fringe Observation.

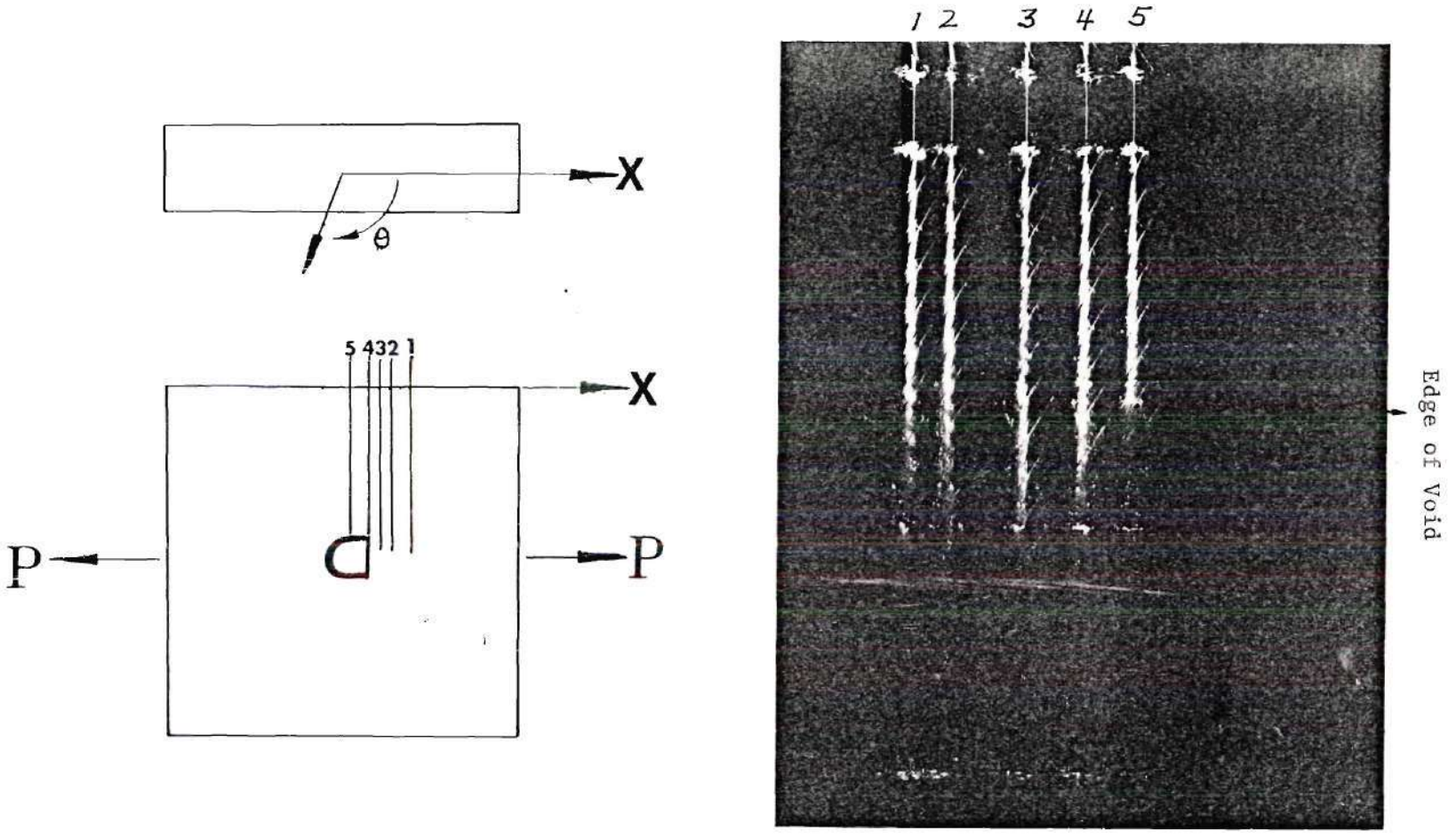

Figure 7a. Fringe Patterns of Different Light Beam Locations When Observation Angle $\theta = 45^{\circ}$.
1:x = 1.00" 2:x = 0.50" 3:x = 0.25" 4"x = 0.00"
5:x = -0.50"

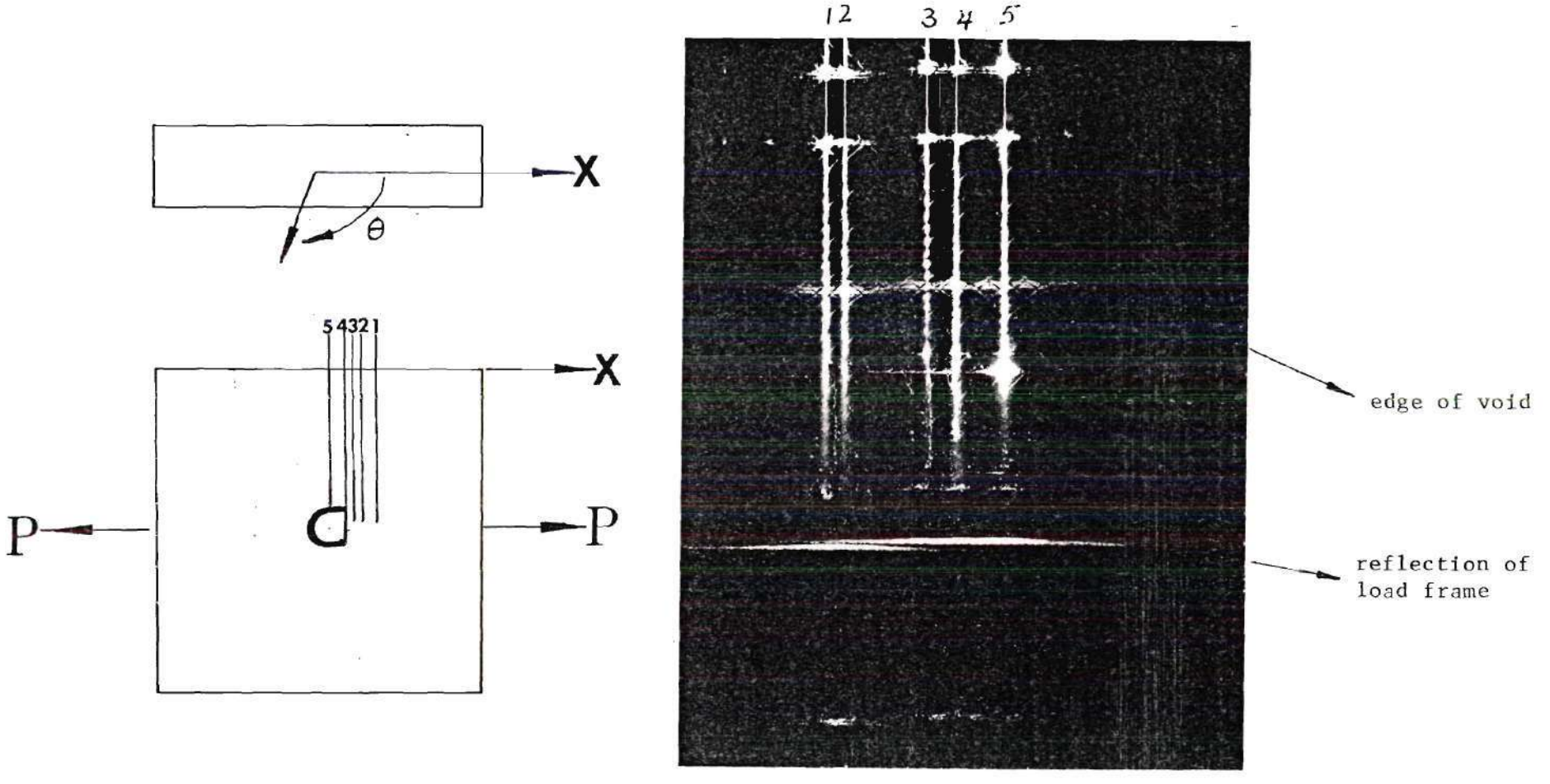

Figure 7b. Fringe Patterns of Different Light Beam Locations When Observation Angle $\theta = 90^{o}$.
1:x = 1.00" 2:x = 0.50" 3:x = 0.25" 4:x = 0.00"
5:x = -0.5"

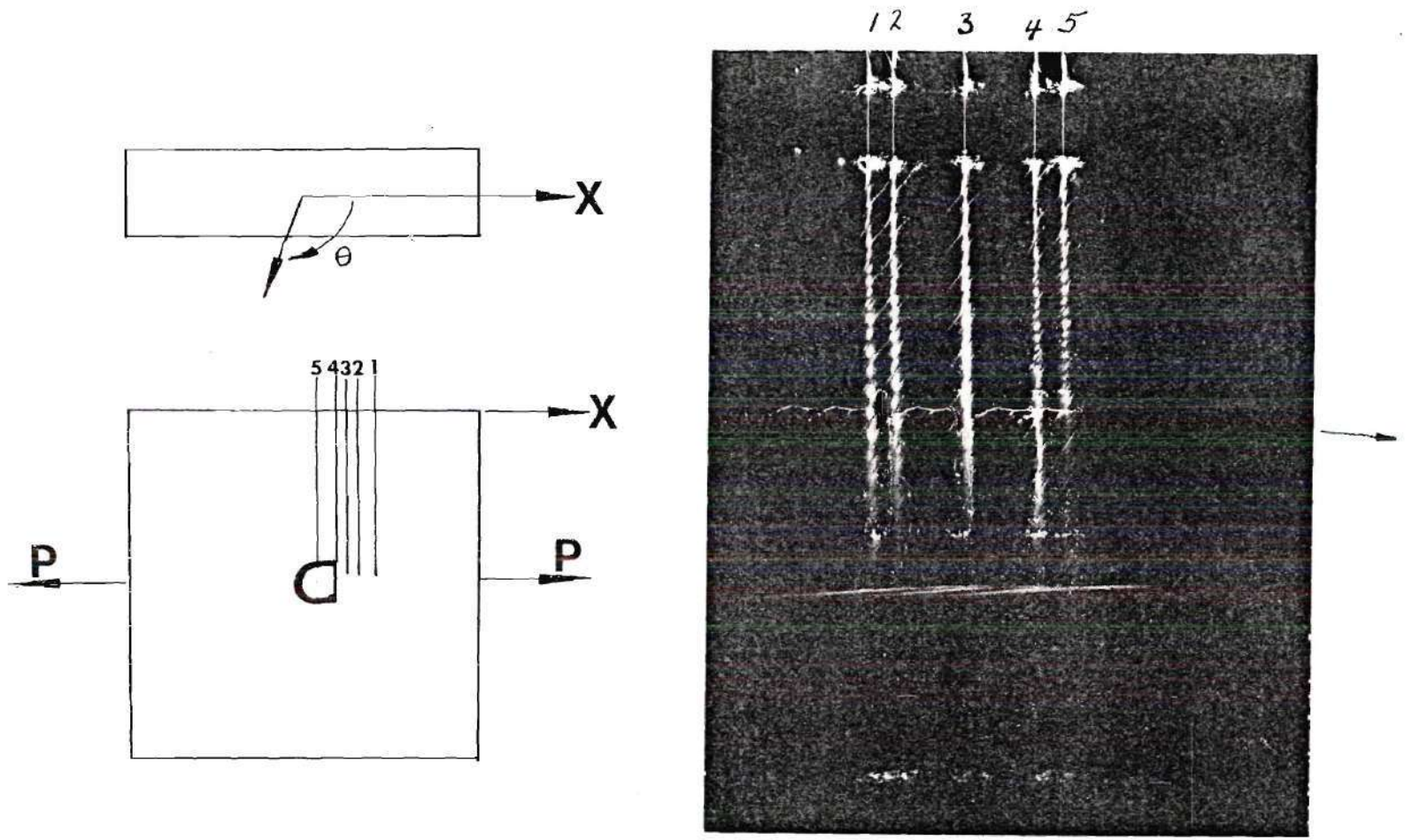

Figure 7c. Fringe Patterns of Different Light Beam Locations When Observation Angle $\theta = 135^{o}$
1:x = 1.00" 2:x = 0.50" 3:x = 0.25" 4:x = 0.00"
5:x = -0.50"

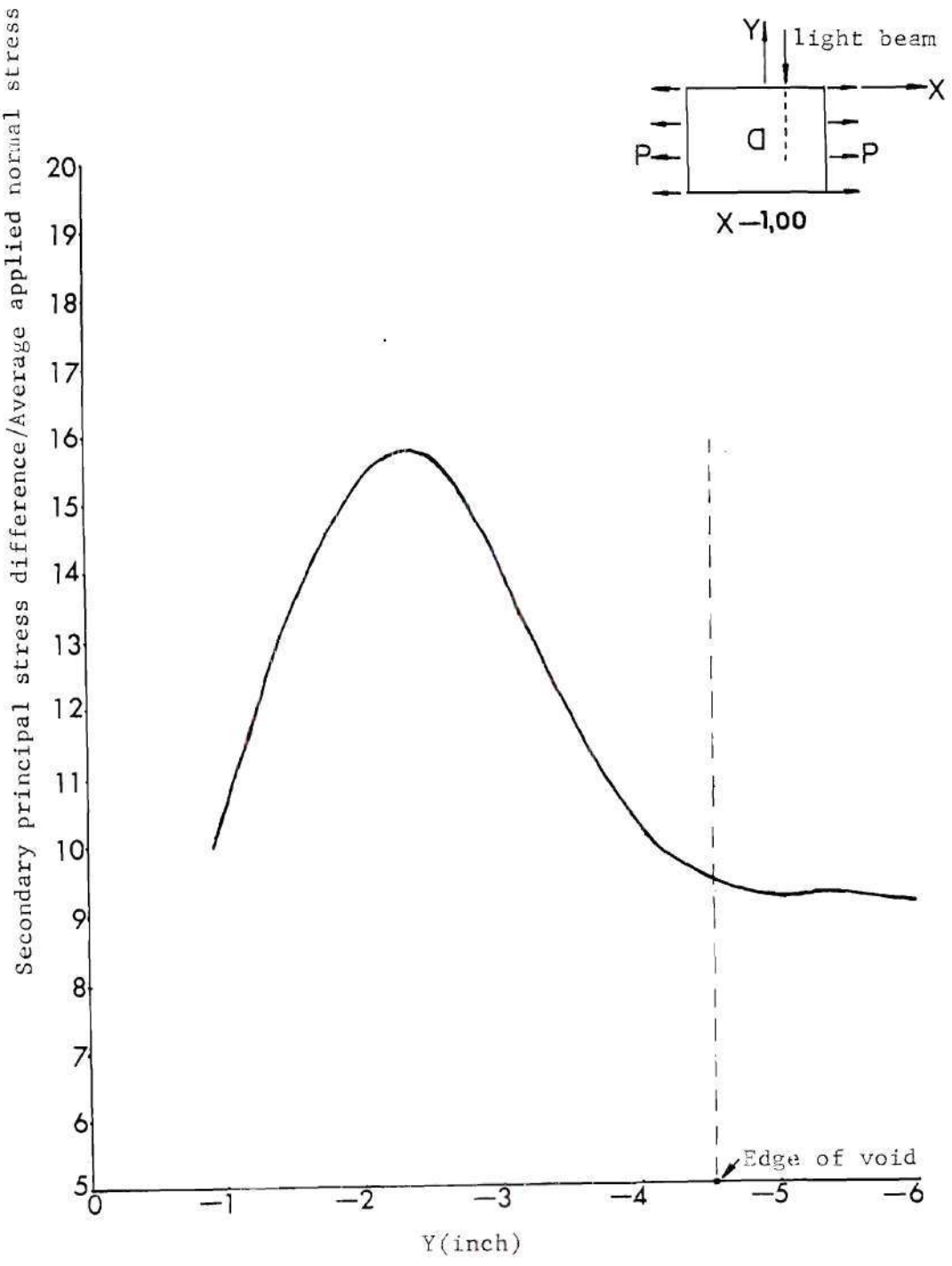

Figure 8a. Interlaminar Secondary Principal Stress Difference in Planes Parallel to Load in the Vicinity of the Void.

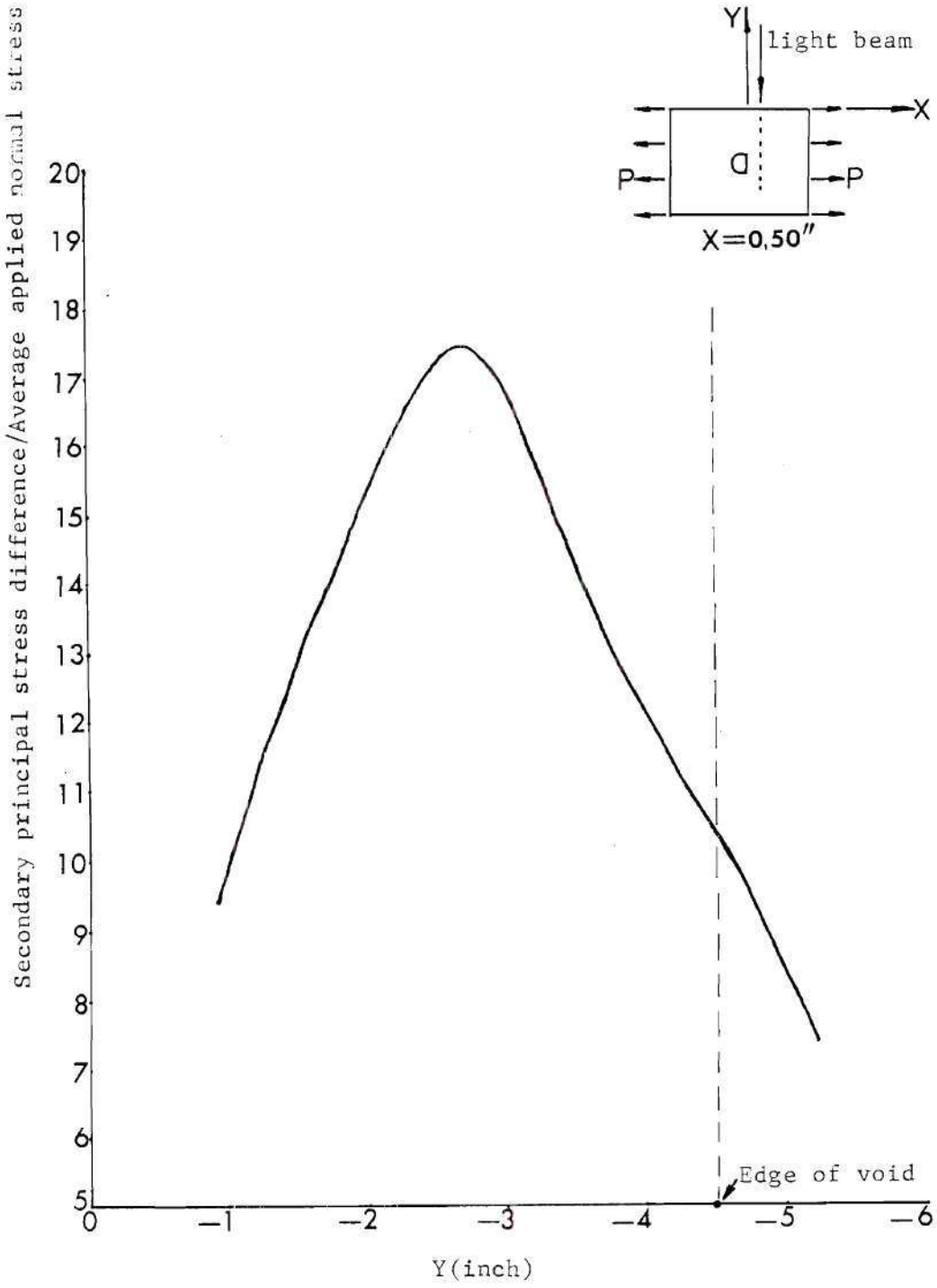

Figure 8b. Interlaminar Secondary Principal Stress Difference in Planes Parallel to Load in the Vicinity of the Void.

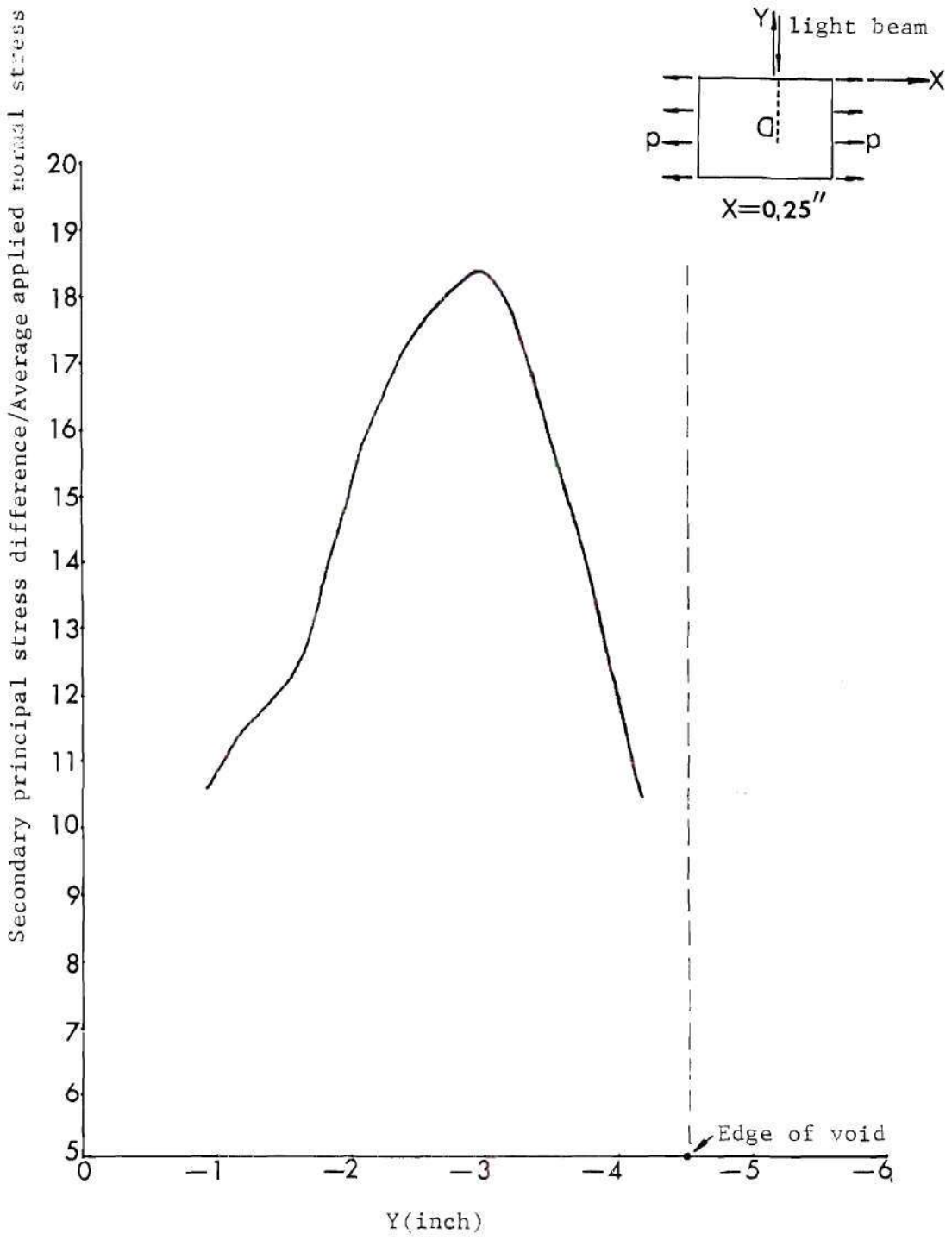

Figure 8c. Interlaminar Secondary Principal Stress Difference in Planes Parallel to Load in the Vicinity of the Void.

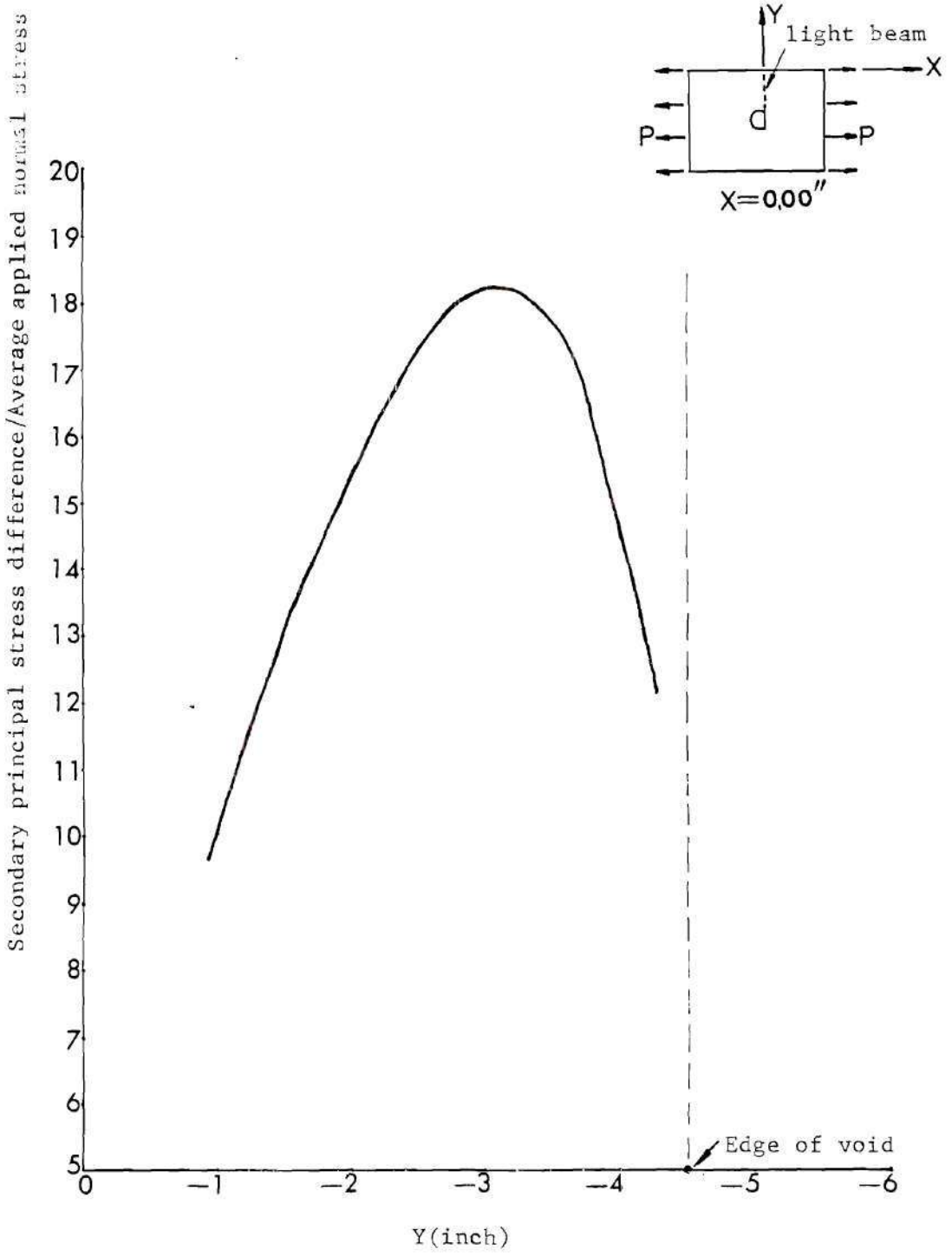

Figure 8d. Interlaminar Secondary Principal Stress Difference in Planes Parallel to Load in the Vicinity of the Void.

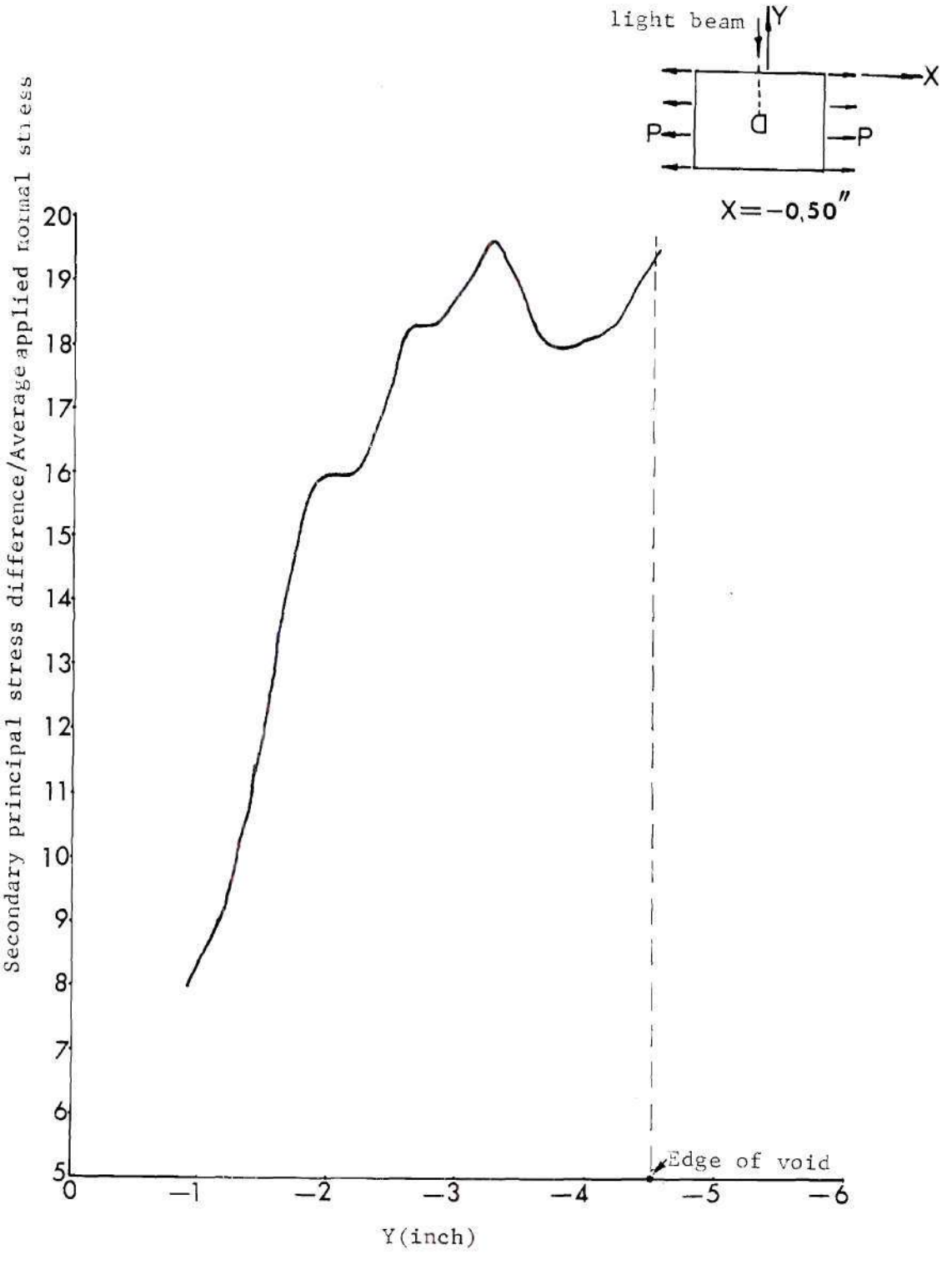

Figure 8e. Interlaminar Secondary Principal Stress Difference in Planes Parallel to Load in the Vicinity of the Void.

BIBLIOGRAPHY

1. Ashton, J. E., Halpin, J. C., and Petit, P. H., "Primer on Composite Materials: Analysis," Technomic Publishing Company, Inc., 1960, p. 30.

2. Sokolnikoff, I. S., "Mathematical Theory of Elasticity," 2nd edition, McGraw-Hall Book Company, Inc., New York, 1956, pp. 56-64.

3. Jones, R. M., "Mechanics of Composite Materials," Scripts Book Company, Washington, D.C., 1975, pp. 147-237.

4. Pipes, R. B., Pagano, N. J., "Interlaminar Stresses in Composite Laminates Under Uniform Axial Extension." Journal Composite Materials, October, 1970, pp. 538-548.

5. Pipes, R. B., Daniel, I. M., "Moiré Analysis of the Interlaminar Shear Edge Effect in Laminated Composites," Journal Composite Materials, April, 1971, pp. 255-259.

6. Belanger, G., "Interlaminar Shear-Delamination Key Factor in Designing Large FRP Tanks," Reinforced Plastic/Composite Institute, The Society of the Plastics Industry, Inc., 28th Annual Technical Conference, 1973.

7. Olster, E. F., "Effect of Voids on Graphite Fiber Reinforced Composite," Final Report, Contract No. 0019-71-C-0305, U. S. Naval Air System Command, Washington, D.C., 1972.

8. Brelant, S., Petker, I., "Fabrication and Environmental Interaction Effects of Filament Wound Composite," from "Mechanics of Composite Materials," F. W. Wendt et al., Eds., Proceedings of the 5th Symposium on Naval Structural Mechanics, Philadelphia 1967, Pergamon Press, New York, 1970, pp. 799-812.

9. Fried, N., "Degradation of Composite Materials: The Effect of Water on Glass-Reinforced Plastics," from "Mechanics of Composite Materials," F. W. Wendt et al., Proceedings of the 5th Symposium on Naval Structural Mechanics, Philadelphia, 1967, Pergamon Press, New York, 1970, pp. 813-840.

10. Cilley, E., Roylance, D., and Schneider, N., "Methods of Fiber and Void Measurement in Graphite/Epoxy Composite," Composite Materials: Testing and Design (Third Conference), ASTM STP 546, American Society for Testing and Materials, 1974, pp. 237-249.

11. Patrick, R. L., "Treatise on Adhesion and Adhesives," Volume 2: Materials, Marcel Dekker, Inc., New York, New York, 1969, pp. 388-401.

12. Owen, D. R. J., Lyness, J. V., "Investigation of Bond Failure in Fibre-Reinforced Materials by the Finite Element Method," Fibre Science and Technology (5) 1972, pp. 129-141.

13. Kavanagh, K. T., "The Effect of Void and Fiber Variations on the Accuracy of Composite Material Characterizations," Journal Composite Materials, October 1973, pp. 500-515.

14. Williams, M. L., "Stress Singularities, Adhesion and Fracture," Proceedings 5th U. S. National Congress Applied Mechanics, June 1966.

15. Daniel, I. M., Rowlands, R. E., and Post, D., "Strain Analysis of Composite by Moiré Method," Experimental Mechanics, 13(b), 1973, pp. 246-252.

16. Dalley, J. W., Alfrevich, J., "Application of Birefringent Coating to Glass-fiber-reinforced Plastics," Experimental Mechanics 3(g), 1969, pp. 97-102.

17. Pipes, R. B., Dalley, J. W., "On the Birefringent-coating Method of Analysis for Fiber-reinforced Laminated Composites," Experimental Mechanics, 12(b), 1972, pp. 272-277.

18. Sutliff, D. R., Pih, H., "Three-Dimensional Scattered-light Stress Analysis of Discontinuous Fiber-reinforced Composites," Experimental Mechanics, July 1973, pp. 294-298.

19. Berghaus, D. G., Aderholdt, R. W., "Photoelastic Analysis of Interlaminar Matrix Stresses in Fibrous Composite Models," Experimental Mechanics, November, 1975, pp. 409-417.

20. Srinath, L. S., Frocht, M. M., "Scattered-light in Photoelasticity-Basic Equipment and Techniques," Proceedings 4th U. S. National Congress of Applied Mechanics, 1972, pp. 775-781.

21. Frocht, M. M., "Photoelasticity," Volume 2, John Wiley and Sons, Inc., New York, 1948, pp. 334-340.

22. Frocht, M. M., Srinath, L. A., "A Non-destructive Method for Three Dimensional Photoelasticity," Proceedings 3rd U. S. National Congress of Applied Mechanics, 1958, pp. 329-337.

23. McKinney, J. M., Swinson, W. F., "Location of Maximum Secondary Principal Axis in Scattered-light Photoelasticity," Proceedings 4th Southeastern Conference for Theoretical and Applied Mechanics, Pergamon Press, 1970.

24. Berghaus, D. G., Cannon, J. P., "Obtaining Derivative from Experimental Data using Smoothed-Spline Functions," Experimental Mechanics 13(1), 1973, pp. 38-42.

25. Sampson, R. C., "A Three Dimensional Photoelastic Method for Analysis of Differential Contraction Stresses," Experimental Mechanics, October 1963, pp. 225-234.

26. Aderholdt, R. W., Berghaus, D. G., "Model Design and Fabrication for Stress Analysis in Multilaminar Composite," Experimental Mechanics, January 1976, pp. 32-37.

27. Frocht, M. M., op. cit. 2, pp. 118-155.